

Effect of Short-Time Aging on the Sensitization Characteristics of 310S Stainless Steel

Guanqun Ma¹, Wen Xian¹, Hongyun Bi², Moucheng Li^{1,*}

¹ Institute of Materials, School of Materials Science and Engineering, Shanghai University, 149 Yanchang Road, Shanghai 200072, China

² Research Institute, Baoshan Iron & Steel Co., Ltd., Shanghai 201900, China

*E-mail: mouchengli@shu.edu.cn

Received: 4 April 2022 / Accepted: 9 May 2022 / Published: 7 August 2022

The sensitization characteristics of 310S stainless steel that was aged at 500 to 900 °C for less than 60 min were investigated by using a double-loop electrochemical potentiokinetic reactivation test (DL-EPR), scanning electron microscopy (SEM) and energy dispersive analysis (EDS). The 310S stainless steel was almost unsensitized after the aging treatments at 600 and 900 °C and was seriously sensitized at 700 and 750 °C. With the increase in aging time from 10 to 60 min, the degree of sensitization changed very slightly after aging at 600 and 900 °C and noticeably enlarged after aging at 700 and 800 °C. The precipitation of carbides during the short-term aging process led to Cr depletion at the grain boundary and then sensitized the 310S specimens.

Keywords: Sensitization, aging, precipitation, 310S stainless steel, intergranular corrosion

1. INTRODUCTION

Currently, electric water heaters are among the most common household appliances. Water-storage type electric water heaters are widely used in daily life due to their low energy consumption and because their characteristics are unaffected by weather [1]. 310S austenitic stainless steel exhibits good high temperature performances and resistance to corrosion due to its high chromium content [2] and is often used as a heating pipe for electric water heaters. However, when electric water heaters are used in regions with poor water quality, internal components, such as heating pipes produced with stainless steels, are prone to corrosion failure in hot tap water environments [3-5].

Stainless steel is sensitized during manufacturing processes, such as welding and annealing treatments in the temperature range of 450 to 900 °C, and the susceptibility to intergranular corrosion must be increased [6-15]. The sensitization mechanisms of stainless steel are mainly related to Cr depletion and the segregation of impurities at the grain boundary. The Cr depletion theory is widely

accepted in practice [16-19]. Due to the supersaturated state in stainless steel, some C atoms combine with metal atoms such as Cr and Fe to form $(\text{Cr, Fe})_{23}\text{C}_6$ carbide during the cooling stage after the solution treatment. The precipitation of carbides at the grain boundaries causes in the formation of a Cr-depleted zone [20,21]. Qian 22 observed the Cr-depletion and C-rich zone at the interface between the M_{23}C_6 carbides and the matrix, which are mainly responsible for the intergranular corrosion of 310S stainless steel at the grain boundaries. Tavares 23 used the double-loop electrochemical potentiokinetic reactivation test (DL-EPR) [24-31] to calculate the sensitization degree (I_r/I_a value) of 310S stainless steel after aging at 600 to 800 °C for 4 to 210 h. The I_r/I_a value increases with aging time for 600 °C but generally reaches a maximum value after a period of aging time (≥ 4 h) for the processes above 650 °C. For the 4 h aging process, the 750 °C temperature may produce the largest I_r/I_a value. The reports [23,32] indicate that prolonged thermal aging contributes to the microstructure instability being self-healed by eliminating the Cr-depletion zone through extensive diffusion of Cr from the matrix. The influence of heat treatment on the sensitization of stainless steel is usually represented by the time-temperature-sensitization (TTS) curve. The TTS curve shows the sensitized and nonsensitized regions [33,34], in which the sensitization temperature within the shortest time can be determined. Based on the intergranular corrosion test results, Parvathavarthini 33 constructed TTS diagrams of the 304 and 316 stainless steels with different degrees of cold work that ranged from 0 to 25%. The nose temperatures of 304 and 316 stainless steels were 650 and 750 °C, respectively. Dománková 34 obtained the TTS curve of 316 stainless steel through an oxalic etching experiment. The fastest sensitization occurred at a nose tip temperature of 800 °C for approximately 20 min.

The 310S stainless steel heating pipe is subjected to high-temperature treatments such as brazing and solution annealing in the manufacturing process. During the cooling process, the heating pipe remains in the sensitization temperature range for a short time. However, the short-term aging effect on the sensitization characteristics of 310S stainless steel is still unclear. In this paper, the sensitization behavior of 310S stainless steel was studied after short-term aging at 500 to 900 °C. The main purpose of the study was to provide fundamental information for the manufacture and application of electric heating tubes.

2. EXPERIMENTAL

2.1 Specimen preparation

A commercial 310S austenitic stainless steel strip with a thickness of approximately 0.4 mm was used as the test material. Table 1 lists the chemical composition of the strip. The steel strips were cut into 10 mm \times 10 mm specimens through wire cutting. A solid solution treatment was conducted for all specimens at 1070 °C for 30 min and then the specimens were quenched in water. Subsequently, the aging treatments of the specimens were carried out at 500 to 900 °C for 10 to 60 min (water quenching).

Table 1. Chemical composition (wt.%) of the 310S austenitic stainless steel

C	Mn	P	Si	Cr	Ni	Mo	N	Ti	Al	Fe
0.04	1.21	0.02	0.74	23.9	19.0	0.01	0.18	0.01	0.02	Bal.

2.2 Double-loop electrochemical potentiokinetic reactivation (DL-EPR) test

The DL-EPR test was performed with a three-electrode system. The saturated calomel electrode (SCE), platinum plate, and specimen were used as the reference electrode, auxiliary electrode, and working electrode, respectively, on a Princeton PMC1000 electrochemical workstation. The test solution was 2 mol L⁻¹ H₂SO₄ + 0.05 mol L⁻¹ KSCN solution at 30 ± 1 °C. For the electrochemical measurements, each specimen was successively ground with 1000 grit SiC paper, welded to a copper wire, and mounted in epoxy resin leaving 1 cm² working area. Prior to each experiment, the working surface is ground with 2000 grit SiC paper, polished with a 1.0 μm diamond polishing agent and cleaned with alcohol and distilled water. Before the DL-EPR test, the specimen was immersed in the electrolyte for 10 min to obtain a nearly steady corrosion state. According to the International Standard ISO 12732:2008, the anodic polarization was conducted from the corrosion potential and returned at 300 mV versus SCE with a scanning rate of 1.667 mV s⁻¹. The electrochemical measurement is repeated at least three times for each type of specimen to confirm its reproducibility.

2.3 Microscopic microstructure and surface characterization

To observe the precipitation phase that was formed during the aging treatment, the specimens were electrolytically etched in a 10 wt.% oxalic acid solution. The intergranular precipitation phase and the specimen surface after the DL-EPR test were analyzed using a Gemini300 scanning electron microscope (SEM) equipped with energy-dispersive X-ray spectroscopy (EDS).

3. RESULTS AND DISCUSSION

3.1 Effect of the aging temperature on the degree of sensitization

Fig.1 shows the typical DL-EPR curves for the specimens after the solid solution treatment and isothermal aging were performed at 500 to 900 °C for 60 min. With increasing electrode potential, the anodic current density in each DL-EPR curve gradually increases, and an activation peak appears at approximately -0.1 V_{SCE}. Subsequently, the current density gradually decreases, indicating that the specimen enters the passivation zone and forms a passive film on the surfaces. During the reverse scanning process, with the continuous decrease in electrode potential to approximately -0.2 V_{SCE}, the passive film dissolves at weak areas such as the grain boundary and Cr-depletion zone, resulting in the formation of a reactivation peak 36. The aging treatment has an insignificant influence on the current

density of the activation peak, with a value of approximately 149 mA cm^{-2} , which is similar to the results in the literature [22,36]. The current density of reactivation peak is approximately $15 \text{ } \mu\text{A cm}^{-2}$ for the solutionized specimen and noticeably increases from approximately 24 to 54 mA cm^{-2} with changing the aging temperature from 500 to $700 \text{ }^\circ\text{C}$ but greatly decreases to approximately $61 \text{ } \mu\text{A cm}^{-2}$ with further increases in the aging temperature from 700 to $900 \text{ }^\circ\text{C}$.

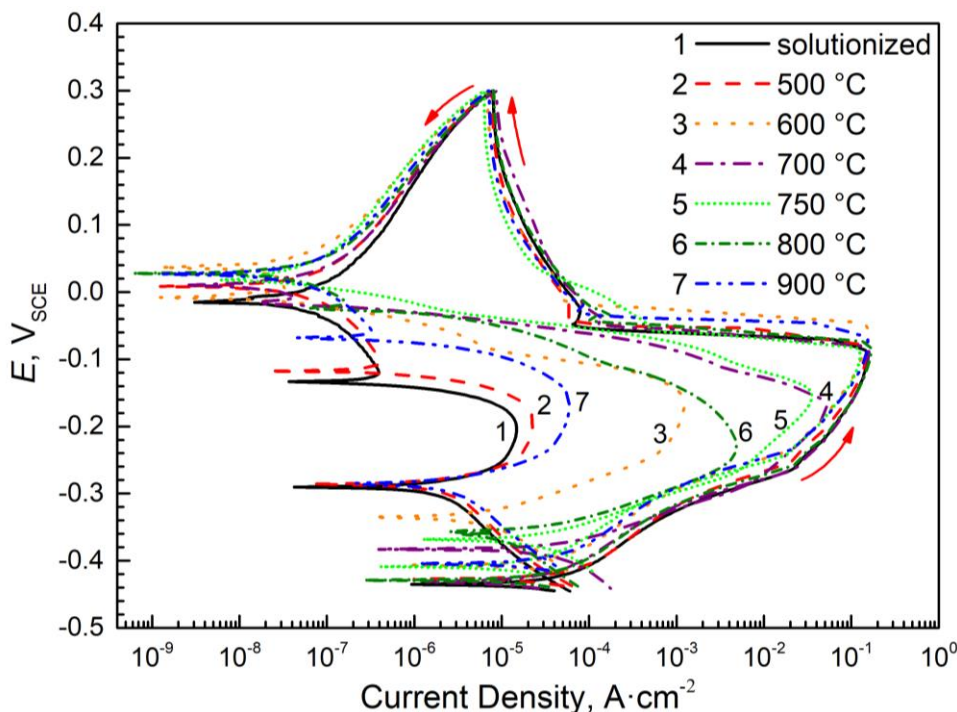


Figure 1. Typical DL-EPR curves in $2 \text{ mol L}^{-1} \text{ H}_2\text{SO}_4 + 0.05 \text{ mol L}^{-1} \text{ KSCN}$ solution at $30 \text{ }^\circ\text{C}$ for the 310S specimens that were solutionized and aged at different temperatures for 60 min. Scan rate 1.667 mV s^{-1}

The degree of sensitization (DOS) of the 310S stainless steel can be calculated with the following equation 35:

$$\text{DOS} = \frac{I_r}{I_a} \times 100\% \tag{1}$$

where I_a and I_r are the current densities of the activation peak and reactivation peak in the DL-EPR curve, respectively. Fig. 2 shows the DOS values of 310S specimens that were aged at various temperatures for 60 min. The DOS value is approximately $0.011 \pm 0.001\%$ for the solutionized specimens. In comparison with the solution treatment, the aging treatment at $500 \text{ }^\circ\text{C}$ has a very slight influence on the DOS value which is approximately $0.015 \pm 0.001 \%$. By changing the aging temperature to 600 and $650 \text{ }^\circ\text{C}$, the DOS values gently increase to $0.75 \pm 0.084 \%$ and $1.01 \pm 0.212\%$, respectively. For the aging treatments at 700 and $750 \text{ }^\circ\text{C}$, the DOS values increase markedly to $33.13 \pm 0.964\%$ and $27.81 \pm 1.16\%$, respectively, which are much higher than in the other cases. With a further increase in the aging temperature to 800 and $900 \text{ }^\circ\text{C}$, the DOS values drop to $2.95 \pm 0.195\%$ and $0.04 \pm 0.004\%$,

respectively. The DOS values are at the same level for the solution treatment and the aging treatments at 500 and 900 °C.

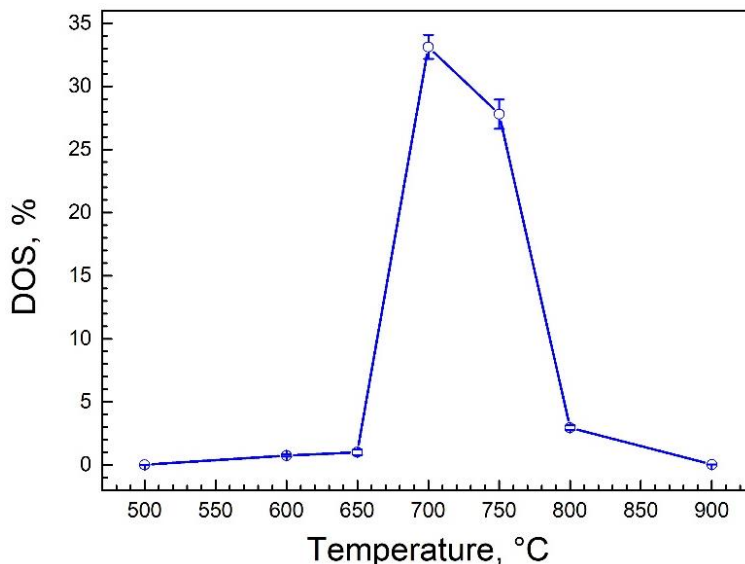


Figure 2. Degree of sensitization (DOS) obtained on the basis of DL-EPR tests for 310S specimens that were aged at 500 to 900 °C for 60 min

Fig. 3 shows the surface morphologies of the specimens after the DL-EPR test. The specimens with the solution treatment and the aging treatments at 500 and 600 °C have similar corrosion surface features, as shown for a typical specimen in Fig. 3(a) for aging at 600 °C. The equiaxed austenite grains and the step structure can be clearly observed on the surfaces according to Standard ASTM-A262, but there is no corrosion ditch at the grain boundaries. After aging at 700 °C in Fig. 3(b) and 750 °C (not provided here), severe intergranular corrosion occurs on the specimen surfaces. The grains are surrounded by corrosion ditches, which are the serious ditch structures according to Standard ASTM-A262. For the specimen that was aged at 800 °C and are shown in Fig. 3(c), the corroded specimen surface displays a dual structure with steps and some discontinuous ditches or small pits at the grain boundaries, but no one grain was completely surrounded by the ditches. The specimens that were aged at 650 °C present corrosion features similar to those observed in Fig. 3(c). As the aging temperature increases to 900 °C, the specimen surface shows very slight traces of corrosion at the grain boundaries in Fig. 3(d).

According to above observation and the suggested correlation of the DOS value with sensitization in the International Standard ISO 12732:2008, it can be concluded that, after 60 min of aging treatment, the 310S stainless steel was almost not sensitized at temperatures 500, 600 and 900 °C, slightly sensitized at 650 and 800 °C, and seriously sensitized at 700 and 750 °C. The aging at 700 °C results in the highest degree of sensitization in comparison with those at other temperatures.

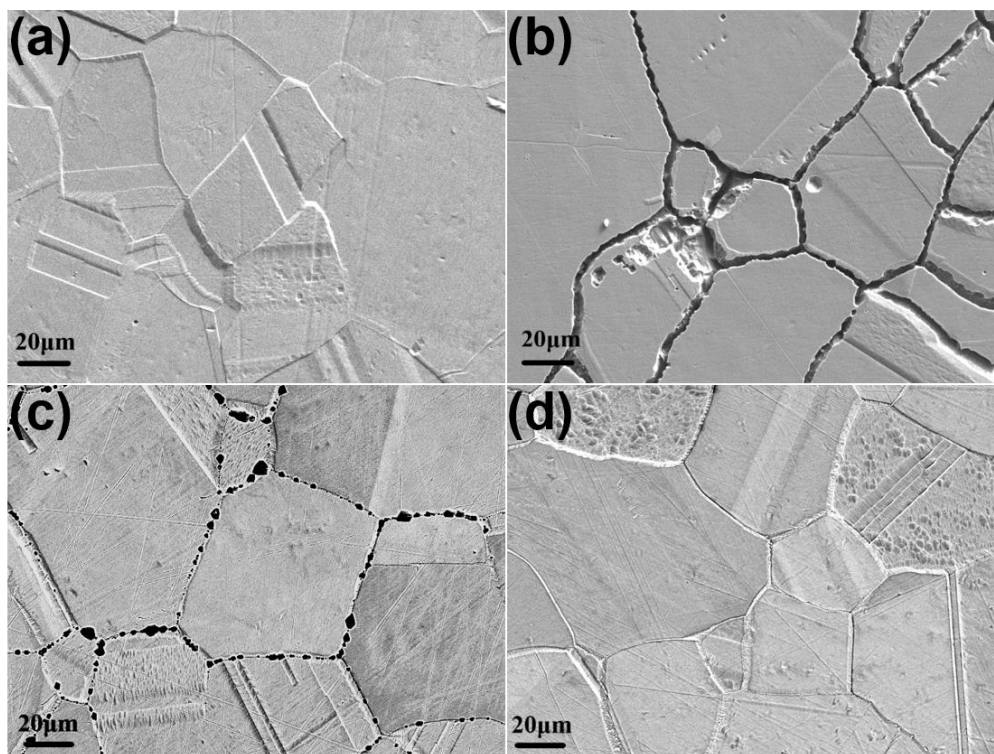


Figure 3. SEM micrographs of surface corrosion morphologies after the DL-EPR test for the 310S specimens that were aged at different temperatures for 60 min: (a) 600 °C, (b) 700 °C, (c) 800 °C and (d) 900 °C.

3.2 Effect of aging time on the degree of sensitization

The aging time is an important factor that influences the sensitization of 310S stainless steel. Fig. 4 provides the DOS values of the specimens that were aged at 500 to 900 °C for different times. The DOS values insignificantly change with aging time and are very small (i.e., less than 0.8%) for the 500, 600 and 900 °C processes. In particular, the 500 and 900 °C treatments resulted in DOS values of less than 0.1%. These values are indicative of the unsensitized states for the specimens aged at the three temperatures. Furthermore, with increasing aging time from 10 to 60 min, the DOS value slightly increases from approximately 0.019% to 0.75% for aging at 600 °C, but decreases from approximately 0.081% to 0.038% for aging at 900 °C. However, the DOS values greatly increase with the aging time for the 700 and 800 °C specimens, especially for the 700 °C treatment which causes the enlargement from $2.40 \pm 0.11\%$ to $33.13 \pm 0.96\%$, which are both larger than the critical value of 1% for the occurrence of sensitization according to Standard ISO 12732:2008. These results indicate that a noticeable increase in the sensitization degree occurs with aging time under the two aging temperature conditions. This is related to the diffusion replenishment rate of Cr at the grain boundary slower than the Cr loss rate caused by carbide precipitation during the short-time aging treatment within 60 min. The gradual increase of DOS value with aging time for the treatments at 600, 700 and 800 °C was also observed on the duplex stainless steels 2507, which is attributed to the precipitation of intergranular

second phase at the grain boundaries [37-38]. However, the DOS value for 310S stainless steel may reach the maxima after aging at 700 and 750 °C for 4 h [23]. The variation of DOS value with time at 900 °C reflects that aging for 10 min is sufficient for Cr diffusion from the grain to the grain boundary. The recovery of Cr content in the depletion zone enhances the intergranular corrosion resistance. This is similar to the sensitization evolution of type 430 stainless steel aged at 800 °C [39].

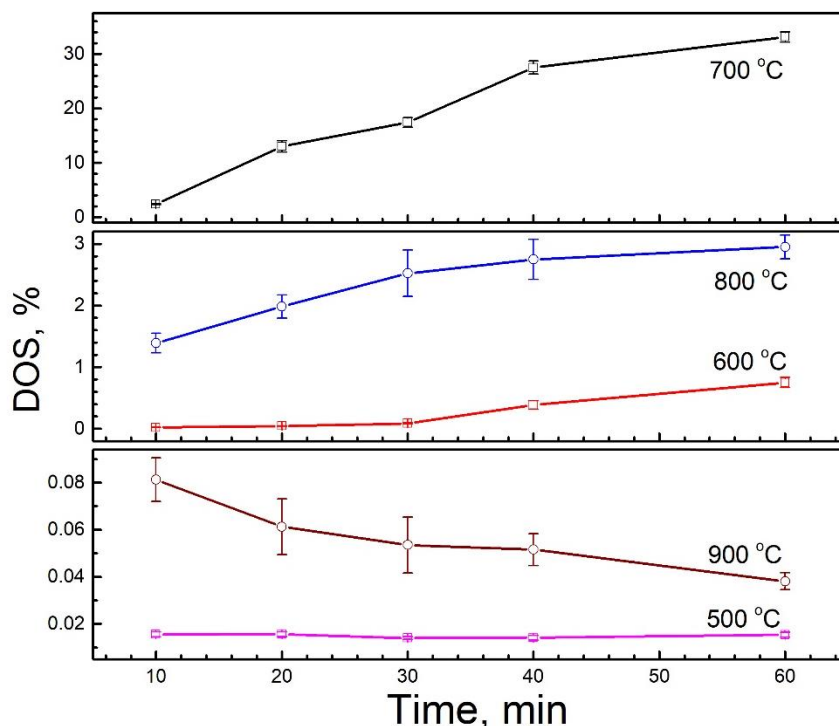


Figure 4. DOS values of the 310S specimens obtained on the basis of DL-EPR tests as a function of aging time at different temperatures from 500 to 900 °C

Fig. 5 shows the typical SEM micrographs of the corrosion morphologies after the DL-EPR test for the 310S specimens that were aged at 700 °C with different times from 10 to 40 min. Fig. 3(b) shows the SEM morphology for the aging time of 60 min. After aging for 10 min in Fig. 5(a), there are shallow steps between the grains and some discontinuous ditches and small pits at the grain boundaries, which is a dual structure according to Standard ASTM-A262. After aging for 20 min, as shown in Fig. 5(b), some continuous corrosion grooves form between the grains but do not surround the grains. After aging for 30 min and longer times in Fig. 5(c, d) and Fig. 3(b), the corrosion becomes more serious. The corrosion ditches gradually surrounded the grains on the specimen surfaces. These results confirm that sensitization takes place for the 310S stainless steel after aging at 700 °C for 10 min and is markedly enhanced with aging time.

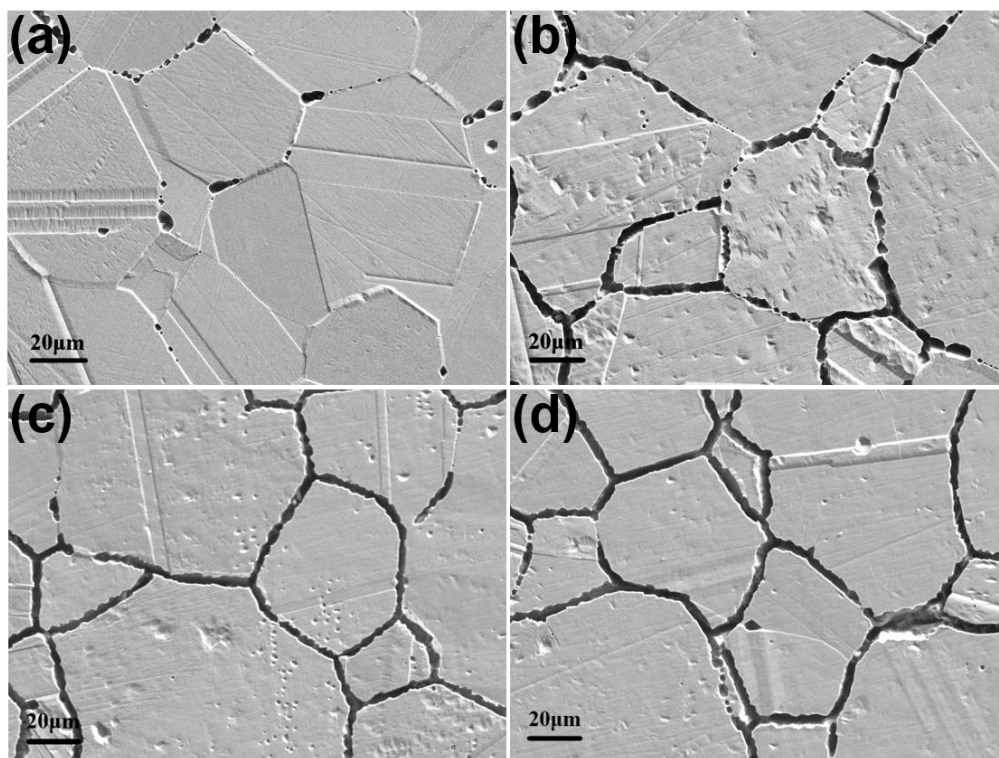


Figure 5. SEM micrographs of surface corrosion morphologies after the DL-EPR test of the specimens that were aged at 700 °C for different times. (a) 10 min, (b) 20 min, (c) 30 min and (d) 40 min.

3.3 XRD analysis

Fig. 6 shows the XRD patterns of the specimens after the solid solution treatment and the aging at 700 °C for 60 min. Both curves present the same response peaks. This indicates that the new phases, such as the precipitates formed in the aging process, cannot be detected by the XRD analysis. The contents of the second phases must be very small in the specimens after they are aged at 700 °C for 60 min despite the appearance of relatively high DOS values.

3.4 Precipitation of carbide

The relatively high free energy at the grain boundary of the material provides the driving force for the solid phase transformation reaction of the second phase precipitation [40]. The 310S specimens that were aged at 700 °C for 10, 30 and 60 min and 800 and 900 °C for 60 min, were electrolytically etched at 4.5 V in the 10 wt.% oxalic acid solution to observe the precipitates. Fig. 7 shows the grain boundary morphologies of these etched specimens.

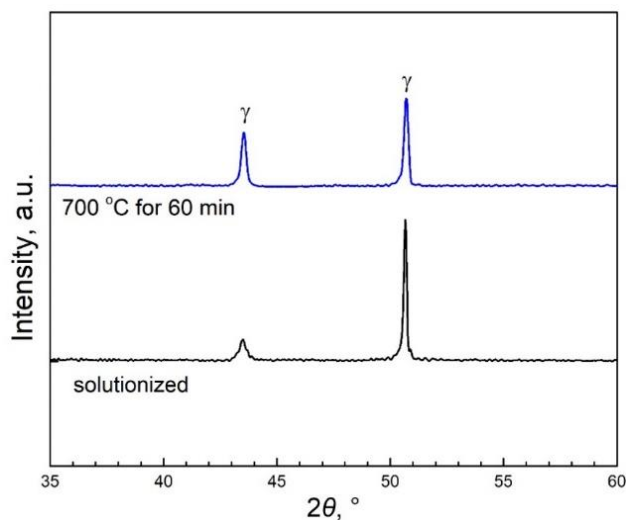


Figure 6. XRD patterns of the specimens after the solution treatment and aging at 700 °C for 60 min

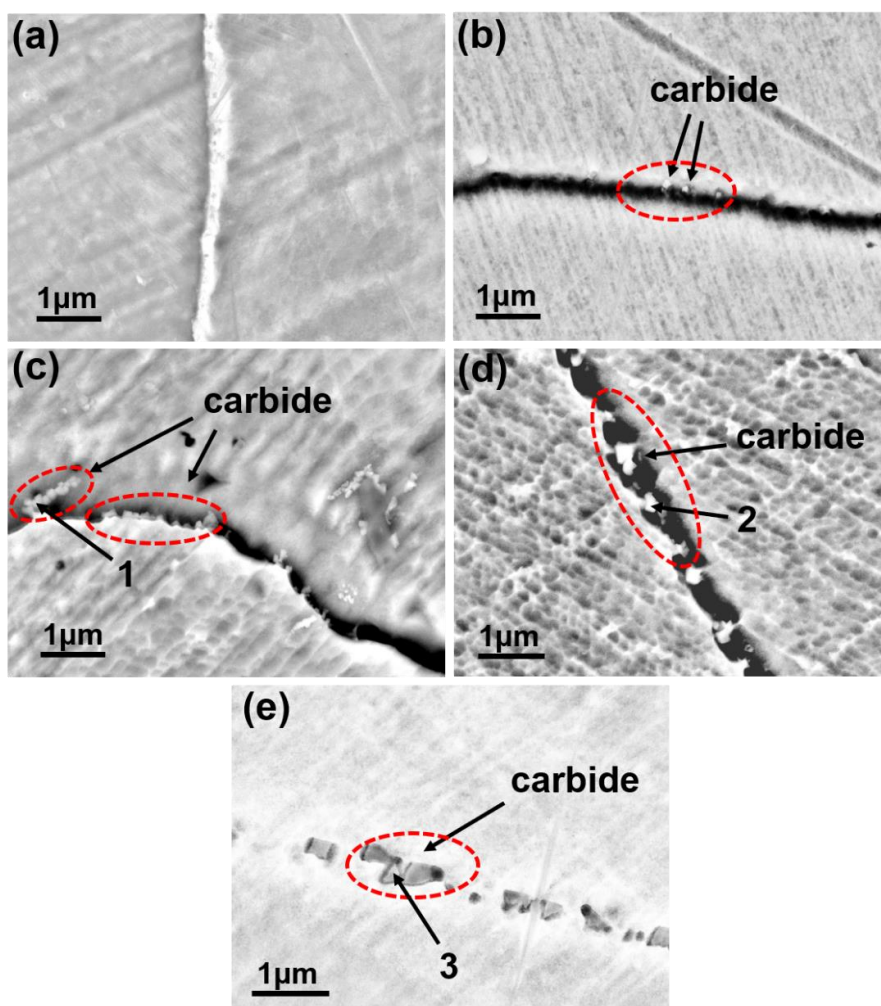


Figure 7. Grain boundary morphologies of the 310S specimens that were aged at 700 °C for (a) 10 min, (b) 30 min and (c) 60 min and at (d) 800 °C and (e) 900 °C for 60 min. (etched at 4.5V in 10 wt.% oxalic acid solution)

It is very difficult to find any precipitates at the grain boundaries in the specimen that were aged at 700 °C for 10 min, as shown in Fig. 7(a). For a longer aging time of 30 min in Fig. 7(b), there are some small precipitates at the grain boundaries of the aged specimen. After aging at 700 °C for 60 min, as shown in Fig. 7(c), the grain boundaries are serrated, and many large precipitates form around the grain boundaries. For the higher aging temperatures at 800 and 900 °C for 60 min, the size of the precipitated phase becomes relatively larger, as shown in Fig. 7(d, e). Table 2 lists the element contents that were detected by EDS analysis at the three positions marked in Fig. 7(c-e). C and Cr are significantly enriched in the precipitates. According to the literature [22,23,41-43], these precipitates are mainly the Cr-rich $M_{23}C_6$ carbide phase.

Table 2. EDS results for element content (wt.%) at the positions marked in Figure 7.

Position	C	Cr	Mn	Fe	Ni
1	9.48	26.76	1.01	46.15	16.6
2	10.32	38.16	1.31	37.76	12.44
3	13.86	26.1	1.28	43.17	15.59

It is apparent that the carbide phase is preferentially precipitated at the grain boundary after the aging of 310S stainless steel. The growth of the $M_{23}C_6$ phase is mainly controlled by the diffusion rate of Cr atoms inside the grains. According to the literature [44,45], the diffusion coefficient D of Cr can be calculated by the following equation:

$$D = D_0 \exp\left(\frac{-Q}{RT}\right) \quad (2)$$

where D_0 is a constant and Q is the activation energy of Cr diffusion. The size of the $M_{23}C_6$ phase (r) can be calculated according to Zener's empirical relation as follows [45]:

$$r = \beta \sqrt{Dt} \quad (3)$$

where β is a constant and t is the aging time. Equation (3) indicates that the carbides may grow with the extension of aging time at a given temperature. Thus, it is seen in Fig. 7(b, c) that the carbide size becomes slightly larger as the aging time is extended from 30 to 60 min at 700 °C. At the same time, these two equations mean that the higher aging temperature facilitates carbide growth due to the larger D value, i.e., the faster Cr diffusion rate. This is responsible for the increase of carbide size with changing aging temperature from 700 to 900 °C, as shown in Fig. 7(c-e).

The carbide precipitation must consume a large amount of Cr elements. Due to the large atomic radius of Cr, the diffusion rate of Cr is much lower than that of C. This means that the Cr consumption at the grain boundary cannot be replenished in a timely manner by the diffusion of Cr from the grain and then inevitably results in forming the Cr-depletion zone along the grain boundary [46,47]. Preferential corrosion may occur along the Cr-depletion zones at the grain boundaries [48-51]. This is the main reason for the appearance of corrosion ditches in Figs. 3, 5, and 7, i.e., the occurrence of sensitization in

the 310S stainless steel. It is clear that the Cr concentration plays an important role in the sensitizing process at the grain boundary, which is related to the aging time as follows [44]:

$$C_{Cr} = C_0 \exp\left(-k \frac{t}{t_{max}}\right) \quad (4)$$

where k is a constant, t is the aging time, t_{max} is the time to achieve complete sensitization at a given temperature, C_0 is the original concentration of Cr, and C_{Cr} is the concentration of Cr after aging for t time. For the relatively low aging temperatures, the diffusion rate of C atoms is too slow to aggregate with Cr atoms at the grain boundaries and form the Cr-depletion zone. This must be the main reason for the insignificant changes in the DOS value with aging time at 500 °C. Under aging temperatures of 600 to 800 °C, the formation of Cr depletion at the grain boundary is controlled by the Cr diffusion process [20]. The Cr atoms in the grain cannot diffuse to the grain boundary in a timely manner. Equation (4) shows that the concentration C_{Cr} gradually decreases with aging time t at a given temperature before reaching complete sensitization. This is mainly responsible for the higher DOS values that are observed after the longer aging treatments at 600 to 800 °C, as seen in Fig. 4. Moreover, it is speculated that the greatest diffusion rate difference between C and Cr atoms may appear at the aging temperature approximately 700 °C, which results in the most serious Cr depletion at the grain boundary and then produces the highest DOS values in comparison with those of the other aging temperatures. A high correlation is well known to exist between the DOS value and the width of the Cr-depletion zone [52]. According to the literature [41], the wider the Cr-depletion zone is, the higher the DOS value. As the aging temperature changes to 800 °C, the difference in diffusion rate between Cr and C atoms may decrease. The Cr atoms in the crystals more easily diffuse to the grain boundaries, which greatly accelerates the healing of the Cr-depletion zone induced by carbide precipitation [23]. When the aging temperature increases to 900 °C, the solubility of C atoms and the diffusion rate of Cr atoms become noticeably higher, which may result in a very small t_{max} value. The Cr atoms in the grains rapidly replenish to the grain boundaries with aging time, which inhibits the depletion of Cr at the grain boundaries. As a result, the DOS value is very small and decreases slightly with aging time.

4. CONCLUSIONS

The sensitization characteristics of 310S stainless steel were studied after aging the steel at 500 to 900 °C for 10 to 60 min. The main conclusions are as follows:

(1) After the aging treatments are performed for 60 min, 310S stainless steel exhibits very low DOS values for the aging temperatures of 500 and 900 °C, which are similar to those for the solution treatment. The DOS value becomes slightly higher with the aging temperature of 600 °C but is still less than 1%. Almost no sensitization occurs for the aging temperatures of 500, 600 and 900 °C. The aging temperatures of 650 and 800 °C result in a slight sensitization for 310S stainless steel with DOS values in the range of 1% to 3%. Under aging temperatures of 700 and 750 °C, serious sensitization is observed in 310S stainless steel with much higher DOS values of approximately 28% to 33%. The highest sensitization degree appears at the aging temperature of 700 °C.

(2) With the increase in aging time from 10 to 60 min, the DOS values are very small (i.e., less than 0.8%) and very slight changes are observed under aging temperatures of 500, 600 and 900 °C. However, the DOS values are higher than the critical value of sensitization and have marked enlargements under aging temperatures of 700 and 800 °C.

(3) Some small carbides appear at the grain boundaries after aging for 30 min at 700 °C and become larger with increasing the aging time to 60 min or the aging temperature. The carbide precipitation results in Cr depletion at the grain boundary, and this depletion is the main factor responsible for the sensitization of 310S stainless steel.

References

1. I. Sezai, L.B.Y. Aldabbagh, U. Atikol and H. Hacisevki, *Appl. Energy*, 81 (2005) 291.
2. Y. Behnamian, A. Mostafaei, A. Kohandehghan, B. S. Amirkhiz, D. Serate, W. Y. Zheng, D. Guzonas, M. Chmielus, W. X. Chen and J. L. Luo, *Mater. Charact.*, 120 (2016) 273.
3. M. J. Zhang., R. H. Xu, L. L. Liu, S. S. Xin and M. C. Li, *Anti-Corros. Methods Mater.*, 67 (2020) 407.
4. Z. Yin, *Int. J. Electrochem. Sci.*, 17 (2022) 2.
5. R. H. Xu, S. S. Xin, Q. Z. Ni, H. T. Zeng and M. C. Li, *Russ. J. Electrochem.*, 57 (2021) 636.
6. A. K. Jha and K. Sreekumar, *Eng. Fail. Anal.*, 16 (2009) 1379.
7. S. G. Chowdhury and R. Singh, *Scr. Mater*, 58 (2008) 1102.
8. A. Y. Kina, V. M. Souza, S. S. M. Tavares, J. A. Souza and H. F. G de Abreu, *J. Mater. Process. Technol.*, 199 (2008) 391.
9. A. Y. Kina, V. M. Souza, S. S. M. Tavares, J. M. Pardal, and J. A. Souza, *Mater. Charact.*, 59 (2008) 651.
10. M. Terada, D. M. Escriba, I. Costa, E. Materna-Morris and A. F. Padilha, *Mater. Charact.*, 59 (2008) 663.
11. E. Bitay and T. Kovács, *Mater. Sci. Forum*, 649 (2010) 107.
12. K. Kaneko, T. Fukunaga, K. Yamada, N. Nakada, M. Kikuchi, Z. Saghi and P. A. Midgley, *Scr. Mater.*, 65 (2011) 509.
13. P. M. Ahmedabadi, V. Kain, B. K. Dangi and I. Samajdar, *Corros. Sci.*, 66 (2013) 242.
14. Y. Zhou and F. A. Yan, *Int. J. Electrochem. Sci.*, 11 (2016) 3976.
15. Xu. L. Y, Li. M, Jing. H. Y and Han. Y. D, *Int. J. Electrochem. Sci.*, 8 (2013) 2069.
16. O. V. Kasparova, *Prot. Met.*, 40 (2004) 425.
17. A. Di Schino and J. M. Kenny, *J. Mater. Sci. Lett.*, 21 (2002) 1969.
18. O. V. Kasparova, *Prot. Met.*, 36 (2000) 524.
19. S. Frangini, *Oxid. Met.*, 53 (2000) 139.
20. T. Sourmail, *Mater. Sci. Technol.*, 17 (2001) 1.
21. H. Sidhom, T. Amadou, H. Sahlaoui and C. Braham, *Metall. Mater. Trans. A*, 38 (2007) 1269.
22. J. Qian, C. F. Chen, H. B. Yu, F. Liu, H. Yang and Z. H. Zhang, *Corros. Sci.*, 111 (2016) 352.
23. S. S. M. Tavares, V. Moura, V. C. Da Costa, M. L. R. Ferreira and J. M. Pardal, *Mater. Charact.*, 60 (2009) 573.
24. P. Záhumenský, S. Tuleja, J. Orszagova, J. Janovec and V. Siládiová, *Corros. Sci.*, 41 (1999) 1305.
25. S. S. M. Tavares, M. P. Fonseca, A. Maia and P. de Lima-Neto, *J. Mater. Sci.*, 38 (2003) 3527.
26. B. Deng, Y. M. Jiang, J. L. Xu, T. Sun, J. Gao, L. H. Zhang, W. Zhang and J. Li, *Corros. Sci.*, 52 (2010) 969.
27. R. Silva, L. F. S. Baroni, M. B. R. Silva, C. R. M. Afonso, S. E. Kuri and C. A. D. Rovere, *Mater. Charact.*, 114 (2016) 211.
28. P. Rosemann, N. Kauss, C. Müller and T. Halle, *Mater. Corros.*, 66 (2015) 1068.

29. J. Gao, Y. M. Jiang, B. Deng, W. Zhang, C. Zhong and J. Li, *Electrochim. Acta*, 54 (2009) 5830.
30. P. Rosemann, C. Müller, N. Kauss and T. Halle, HTM, *J. Heat Treat. Mater.*, 72 (2017) 87.
31. N. Lopez, M. Cid, M. Puiggali, I. Azkarate and A. Pelayo, *Mater. Sci. Eng., A*, 229 (1997) 123.
32. A. Kriaa, N. Hamdi and H. Sidhom, *Prot. Met.*, 44 (2008) 506.
33. N. Parvathavarthini, R. K. Dayal, S. K. Seshadri and J. B. Gnanamoorthy, *J. Nucl. Mater.*, 168 (1989) 83.
34. M. Dománková, E. Kocsisová, I. Slatkovský and P. Pinke, *Acta. Polytech. Hung.*, 11 (2014) 125.
35. S. D. Ban, Y. T. Shin, S. R. Lee and H. W. Lee, *Int. J. Electrochem. Sci.*, 11 (2016) 7764.
36. G. H. Aydoğdu and M. K. Aydinol, *Corros. Sci.*, 48 (2006) 3565.
37. L. Sun, Y. T. Sun, C. X. Lv, Y. Y. Liu, N. W. Dai, Y. M. Jiang, J. Li and D.D. Macdonald, *Corros. Sci.*, 185 (2021) 109432
38. J. F. Hong, D. Han, H. Tan, J. Li and Y. M. Jiang, *Corros. Sci.*, 68 (2013) 249.
39. A. S. M. Paroni, N. Alonso-Falleiros and R. Magnabosco, *Corrosion*, 62 (2006) 1039.
40. I. Le May and W. E. White, *Metallography*, 5 (1972) 566.
41. Y. Jiao, J. Mahmood, W. Zheng, P. M. Singh and J. R. Kish, *Corrosion*, 74 (2018) 430.
42. R. L. Cowan and C. S. Tedmon, *Adv. Corros. Sci. Technol.*, 3 (1973) 293.
43. Y. N. Jiao, W. Y. Zheng and J. R. Kish, *Corros. Sci.*, 135 (2018) 1.
44. W. E. Mayo, *Mater. Sci. Eng., A*, 232 (1997) 129.
45. H. Sahlaoui, H. Sidhom and J. Philibert, *Acta Mater.*, 50 (2002) 1383.
46. F. F. Curiel, R. García, V. H. López, M. A. García, A. Contreras and M. A. García, *Int. J. Electrochem. Sci.*, 16 (2021) 1.
47. C. Y. Yuh, L. Chen, A. Franco and M. Farooque, *Int. Conf. Fuel Cell Sci., Eng., Technol.*, 44052 (2010) 387.
48. T. Sourmail, C. H. Too, H. K. D. H. Bhadeshia, *ISIJ Int.*, 43 (2003) 1814.
49. V. Vignal, S. Ringeval, S. Thiébaud, K. Tabalaiev, C. Dessolin, O. Heintz and R. Chassagnon, *Corros. Sci.*, 85 (2014) 42.
50. S. Y. Lu, K. F. Yao, Y. B. Chen, M. H. Wang, N. Chen and X. Y. Ge, *Corros. Sci.*, 103 (2016) 95.
51. Y. Hou, C. Q. Cheng, T. S. Cao, X. H. Min and J. Zhao, *Int. J. Electrochem. Sci.*, 13 (2018) 7095.
52. S. M. Bruemmer, L. A. Chariot and B. W. Arey, *Corrosion*, 44 (1988) 328.